Embedded Model Control: Application to Web Winding. Part II: Digital Control

Conference Paper · September 2006

DOI: 10.1109/ETFA.2006.355345 · Source: DBLP

2 authors:

Enrico Canuto
Politecnico di Torino Former Faculty
227 PUBLICATIONS **2,011** CITATIONS
SEE PROFILE

Fabio Musso
Thales Group
30 PUBLICATIONS **163** CITATIONS
SEE PROFILE

Available online at www.sciencedirect.com
ScienceDirect
ISA Transactions 46 (2007) 379–390
www.elsevier.com/locate/isatrans

Embedded model control: Application to web winding

Enrico Canuto*, Fabio Musso

Politecnico di Torino, Dipartimento di Automatica e Informatica, Corso Duca degli Abruzzi 24, 10129 Torino, Italy

Received 12 July 2006; accepted 19 January 2007
Available online 6 April 2007

Abstract

Embedded Model Control (EMC) methodology is applied to web-winding control problems. These require time-varying Embedded Model and adaptive control law, because of a variable winder radius; disturbance estimation and rejection, because of friction and variable web speed and acceleration; sensorless reel radius estimation; and robust stability and performance in the presence of web and gear vibrations. The goal is to solve these key issues in the framework of EMC, which amounts to (i) designing a time-varying Control Law capable of disturbance rejection, (ii) designing Noise Estimators capable of keeping live and accurate disturbance and radius estimates, and (iii) tuning their eigenvalues to guarantee stability and performance. Tuning takes advantage of an 'error loop' formulation, which explicitly relates neglected dynamics to eigenvalues, stability and performance. Simulated runs from a fine winder model are compared to published results.

Keywords: Process control; Modeling; Web winding; Digital control; Embedded model

1. Introduction

Automatic tension control in web winding and unwinding processes is one of the most classical control problems. Control design of a full unwinding–traction–winding apparatus, or just of the winding and unwinding sections, although widely treated [1–4], must still be considered a challenging problem due to coupling between tension and line speed, time variability of many process parameters and the presence of not negligible nonlinearity. Industrial experience shows that traditional decentralized PID controls are difficult to set up and subject to performance degradation. To overcome such difficulties, attention has been paid to modeling web and roll dynamics [2,4–8]. The goal is to dispose of mathematical models, thus allowing direct design and tuning of robust control strategies, which are expected to reduce in-field set-up times. Notwithstanding these efforts, some key issues still appear open.

(1) Design models are linear, so that they may be identified from experimental data [2,4,6] and enable linear design techniques, like Linear Quadratic Gaussian (LQG) control [4] and H_∞ [2]. Variable reel radius may be accounted for in the linear control law by gain-scheduling techniques [3]. Here, the design model explicitly allows for a variable reel radius, enabling model and control adaptation (Section 3.2).
(2) Sensorless reel radius measurement, i.e. without relying on ad-hoc sensors, has been studied, but only in the open-loop form [9], hence subject to unbounded drift. Here a hybrid state observer, operating in closed-loop under winding conditions (see Section 4.3.2), ensures a bounded estimation error.
(3) Little attention has been paid to formulating discrepancies and uncertainties of the real plant in terms of a design model and a finer model, which is a key point to assess stability and performance robustness a priori.
(4) Likewise little work has been done in formulating disturbance dynamics in the design model, which is the key toward direct rejection of disturbances. Some work in this direction can be found in [9] where friction is modeled and estimated for this purpose. Here a more generic approach is followed, independent of phenomena and parameters. Variable and complex disturbances like friction are cast into a class of arbitrary and unknown noise-driven signals.

The Embedded Model Control (EMC) outlined in [10] and applied here, has been found capable of addressing previous

* Corresponding author. Tel.: +39 011 564 7026; fax: +39 011 564 7099.
E-mail address: enrico.canuto@polito.it (E. Canuto).

0019-0578/$ - see front matter © 2007, ISA. Published by Elsevier Ltd. All rights reserved.
doi:10.1016/j.isatra.2007.01.002

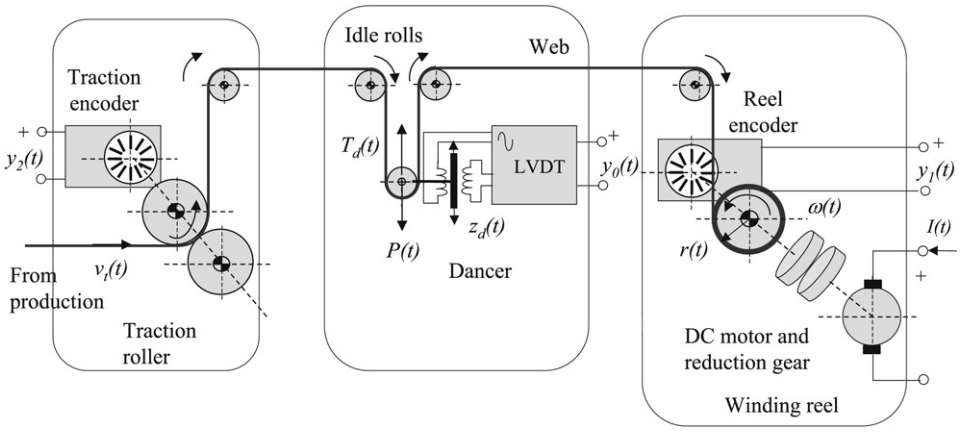

Fig. 1. Winder and dancer layout.

issues which do pertain not only to winding processes. The paper is organized as follows. Section 2 briefly reports the basic assumptions leading to the winder fine model, partly available in the literature [8]. The aim is to justify the simplifications leading to the Embedded Model (EM) in Section 3 and to the subsequent neglected dynamics. The Embedded Model is here extended to include reel radius dynamics. The paper is limited to winding plants where the reference tension is imposed by a dancer roll [1]. Section 4 applies EMC to univariate Control Law and to multivariate Noise Estimator of winding processes. The algorithm demonstrated in [10] is shown to remain valid for variable radius. The latter algorithm is extended to a sensorless reel radius estimator and adaptive control. Section 5 takes advantage of the error loop formulation in [10] to provide the analytic tuning of Control Law and Noise Estimator eigenvalues. Section 6 discusses the EMC performance, recorded from extensive runs on the simulated fine model of Section 2, and compares it to published reports [9].

2. Fine model of the winder

A description of web winding processes is given together with assumptions leading to the fine model detailed below. The simulated fine model is employed as a test-bench for control design and tuning prior to and during in-field tests. Further simplifications outlined in Sections 2.5 and 3.2 lead to separating EM and neglected dynamics.

2.1. Assumptions

The analysis is limited to a winding section such as that in Fig. 1, which is situated between a traction roller, $j = 6$, and a winding reel, $j = 0$, to be commanded by a control unit. The traction roller is moved by its own electric motor, which is outside the analysis and design. Deviations of the web tension from the reference value that is implemented by a vertical force $-P$ on the dancer roll, $j = 3$, affect the dancer vertical position z_d. The measure of z_d becomes the variable to be controlled. Dancer roll may be replaced by load cells [1] directly measuring the web tension on some idle rolls. A pair of idle rolls $j = 5, 4$, transports web from traction roller to dancer roll, and another pair, $j = 2, 1$, from dancer roll to reel. The reel is moved by a DC motor through a reduction gear. The motor current I is driven by the control unit through a current-regulated power amplifier affected by delay and noise.

The fine model is based on less restrictive assumptions than [8], and while neglecting the uncontrollable lateral motion, it details critical dynamics of the controllable tangential motion.

(1) Unlike what occurs in [8], which only treats rollers driven by motor, each web span j comprised between two consecutive rolls $j + 1$ and j is separately described as it contributes to overall dynamics with specific vibration modes.

(2) The web material is in contact with each roller $j = 0, \ldots, 6$ through an adhesion arc θ_{aj} at the beginning of the contact arc θ_{cj}, where tension is constant and equal to T_j and the web velocity v_j equals the tangential velocity at the roller surface. The tangential position x_j defined by $\dot{x}_j(t) = v_j(t)$ accounts for the length of the web passing through an arbitrary point of the adhesion arc from an initial time t_0. Velocity v_j and position x_j are selected as the state variables of the idle rolls $j = 1, 2, 4, 5$ and of the dancer roll $j = 3$. Unlike what occurs in [8], partial slippage between web material and idle rolls cannot be neglected: it takes place at the end of the contact arc along a variable slippage arc $\theta_{sj} = \theta_{cj} - \theta_{aj} < \theta_{cj}$ where tension increases from T_j up to T_{j-1} to balance roll inertia and friction torques. Partial slippage, corresponding to

$$\theta_{sj} = \ln\left(T_{j-1}/T_j\right)/f_j < \theta_{cj}, \tag{1}$$

is ensured by an adequate surface friction coefficient f_j and by the control itself, as far as sharp acceleration is avoided. The dancer roll, subject to reference tension P, web tensions and friction $A_d(v_d)$, is free to move along the vertical axis and as such it requires further state variables: z_d and the vertical speed $v_d = \dot{z}_d$.

(3) As in [8], (i) web strain is assumed to be very small, $\varepsilon_j \ll 1$, and uniform across the web span; (ii) temperature and humidity are assumed not to change; (iii) there is no change in the density ρ and in the modulus of elasticity

E along the web span, nor does the web cross-sectional area $S = L\underline{s}$ change, L being the constant width across the winding section and $\underline{s}$ the mean web thickness, very small compared to the radius of rollers as in [8]. This entails the length l_j of the free web span j being treated as constant and equal to the length at rest $l_j = l_{j0}$, except for the web spans $j = 2, 3$ located upward and downward of the dancer roll. In this case l_j depends on the dancer displacement z_d and on the web inclination α_j with respect to the horizontal axis. Assuming $\alpha_j = \pi/2$, for simplicity's sake, implies $l_j = l_{j0} - z_d$, $j = 2, 3$. The strain is then defined as

$$\begin{aligned} \varepsilon_j(t) &= \left(x_j(t) - x_{j+1}(t)\right)/l_j, \quad j = 0, 1, 4, 5 \\ \varepsilon_j(t) &= \left(x_j(t) - z_d(t) - x_{j+1}(t)\right)/l_j(t), \quad j = 2, 3, \end{aligned} \tag{2}$$

and similar equations pertain to strain rate $\dot{\varepsilon}_j$.

(4) The free web span j is assumed free of mass and subject to the tension T_j, positive in the winding direction. T_j accounts for elastic strain and viscosity, not mentioned in [8], through constant elastic and viscous coefficients per unit length $k = ES$[N] and f[N s], independent of the web span. The web tension holds

$$T_j(t) = k\varepsilon_j(t) + f\dot{\varepsilon}_j(t). \tag{3}$$

(5) The mass of each web span $j-1$ is added to the mass m_j of the upward roll j according to $m_j(t) = J_j/r_j^2 + \mu_0 l_{j-1}(t)$, where J_j and r_j denote constant inertia and radius of the roll, respectively, and $\mu_0 = S\rho$ is the linear mass density of the web. Note that m_j may change with l_j unlike in [8]. Roll j is also subject to friction tangential forces $A_j\left(v_j\right)$.

(6) The tangential position $x_t = x_6$ is the only state variable of the traction roller, the velocity $v_t = r_t\omega_t$ being treated below as an external disturbance.

(7) The ensemble comprising winding reel and wound web is assumed to be a rotating rigid body affected by variable eccentricity η_r. Its tangential position x_0 is related to reel radius r and angular velocity ω by $\dot{x}(t) = r(t)\omega(t)$. Unlike in [8], change in web thickness $s_0(t)$ due to transverse strain is explicitly modeled in order to accurately compute r. Denoting Poisson ratio with ν, it turns out that $s_0(t) = \underline{s}(1 - \nu T_0(t)/(ES))$. The radius r is then defined as follows

$$\dot{r}(t) = 0.5s(t)\omega(t)/\pi, \qquad r(t_0) = r_0 > 0. \tag{4}$$

The reel inertia J_r and mass m_r depend on r through the well-known formulae

$$\begin{aligned} J_r(t) &= J_{r0} + 0.5\rho L\pi(r^4(t) - r_0^4) \\ m_r(t) &= m_{r0} + \rho L\pi(r^2(t) - r_0^2). \end{aligned} \tag{5}$$

(8) The reduction gear between motor and reel is subject to torsional deformation. The torque transmitted from gear to reel is defined by $C_r = K_r(\theta_m/\tau - x_0/r)$, where τ is the gear reduction and θ_m is the angular position of the driving DC motor. DC motor and gear are treated as a single rigid body with angular rate $\omega_m = \dot{\theta}_m$ and inertia J_m. Losses are described by a friction torque $A_m(\omega_m)$ and the motor torque holds $C_m = \phi I$, ϕ being the motor flux [V s]. The DC motor is supplied by a current-regulated amplifier having voltage-to-current gain A, time delay τ_a and noise w_a.

(9) Friction affecting dancer, rolls, reel, gear and DC motor is accurately modeled through static speed-to-friction relations similar to [9], up to scale factors.

Table 1
Web and winder properties

Parameter		Symbol	Unit	Value
Density		ρ	kg/m^3	2740
Width		L	m	1
Young's modulus		E	N/m^2	2×10^9
Mean thickness		$\underline{s}$	m	50×10^{-6}
Empty reel radius		r_0	m	0.15
Empty reel inertia		J_{r0}	kg m^2	21
Reel eccentricity		η_r	mm	<0.2
Mean reel-to-dancer web length			m	2.25
Total dancer moving mass		m_d	kg	148
Reel DC motor	Rated torque		N m	270
	Coulomb friction		N m	<25

2.2. State equations

The above assumptions lead to a set of $n = 18$ nonlinear continuous-time state equations, listed below. Input variables are the amplifier voltage V_a as a command, the traction speed v_t and the reference tension P as disturbances.

(1) Winding reel

$$\begin{aligned} \dot{x}_0(t) &= r(t)\omega(t) \\ \dot{\omega}(t) &= (C_r(t) - (T_0(t) + A_0(\dot{x}_0))r(t) \\ &\quad - gm_r(r)\eta_r(t)\cos(x_0/r - \theta_0))/J_r(r) \\ \dot{r}(t) &= 0.5s(t)\omega(t)/\pi. \end{aligned} \tag{6}$$

(2) DC motor, gear and amplifier

$$\begin{aligned} \dot{\theta}_m(t) &= \omega_m(t) \\ \dot{\omega}_m(t) &= (\phi I(t) - C_r(t) - A_m(\omega_m))/J_m \\ I(t) &= A(V_a(t - \tau_a) + w_a(t)). \end{aligned} \tag{7}$$

(3) Dancer vertical motion

$$\begin{aligned} \dot{z}_d(t) &= v_d(t) \\ \dot{v}_d(t) &= (-P(t) + T_2(t) + T_3(t) - A_d(v_d))/m_d. \end{aligned} \tag{8}$$

(4) Idle and dancer rolls tangential motion

$$\begin{aligned} \dot{z}_j(t) &= v_j(t), \quad j = 1, \ldots, 5 \\ \dot{v}_j(t) &= \left(T_{j-1}(t) - T_j(t) - A_j\left(v_j\right)\right)/m_j. \end{aligned} \tag{9}$$

(5) Traction roller

$$\dot{x}_t(t) = v_t(t). \tag{10}$$

Simulation and control design assume the web and DC motor properties in Table 1, which are comparable to [8].

2.3. Winder measurements

Three winder variables must be measured to ensure the Embedded Model is observable, as proved in Section 3.3.

(1) The traction roller angular speed $\omega_t = v_t/r_t$ is measured by an incremental encoder on the roller shaft, r_t denoting the roller radius.
(2) The reel angular speed ω_r is measured by an incremental encoder on the reel shaft.
(3) The dancer vertical position z_d is measured by a linear variable differential transformer (LVDT).

As in [8], sensor dynamics is considered to be negligible compared to the process dynamics detailed above. Sensor quantization is designed in Section 5. Encoder quantization is defined by the counts per revolution $4N_x$, $N_x, x = r, t$, being the optical slot count. LVDT quantization is defined by sensor range $z_{d,\max}$ and ADC bit number μ_d.

2.4. Disturbance class and uncertainties

Uncertainties are due to disturbance and parameters. First of all disturbance uncertainty is formulated in the discrete-time domain, as any actual wide-band noise, being band-limited, can be carefully approximated by a DT white noise below cutoff frequency. Therefore any disturbance class results from a DT state equation driven by a bounded set of initial states and a class of arbitrary, bounded signals, usually formulated as a DT white noise.

Consider the traction speed $v_t = x_{20}$, tracking after some delay, a reference $\underline{v}_t$, while respecting rate, acceleration and jerk bounds of the typical maneuvers of web processes. The resulting velocity profiles, behaving like smooth steps as in Fig. 5, are the output of the second order dynamics

$$\begin{aligned} x_{20}(i+1) &= x_{20}(i) + x_{21}(i) + w_{20}(i) \\ x_{21}(i+1) &= x_{21}(i) + s_t(i) \\ s_t(i) &= F_t\left(x_{20}(i), x_{21}(i), \underline{v}_t(i)\right) + w_{21}(i), \end{aligned} \tag{11}$$

driven by the nonlinear feedback $F_t(\cdot)$, capable of respecting bounds and emulating the traction controller. In (11), $a_t = x_{21}$ and s_t denote acceleration and jerk in speed units [m/s]. The white noise w_{20} and w_{21} accounts for deviations from feedback law. The same dynamics as in (11) is adopted by the EM, although cast in a wider formulation arising from assuming jerk as a DT white noise:

$$s_t(i) = w_{21}(i). \tag{12}$$

A similar but simpler formulation applies to the reference tension, described as a bounded mean value $0 \le P_0 \le \bar{P}_0$ corrupted by a noise $w_p(i)$ as follows

$$P(i) = P_0 + w_p(i). \tag{13}$$

2.5. From fine model to EM

The fine model is developed aiming at a test-bench capable of enlightening all critical issues of the real dynamics which may affect closed-loop stability and performance.

(1) *Plant variability*. The main source is the reel radius r varying during web winding. It will be explicitly accounted for in the Embedded Model.

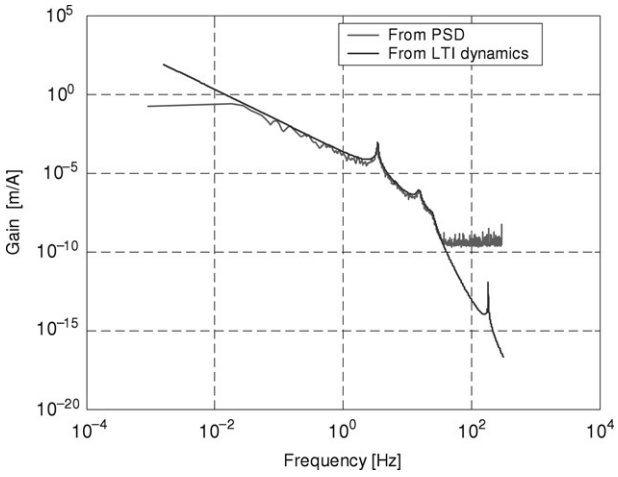

Fig. 2. Analytic and simulated harmonic response of z_d.

(2) *Unknown disturbances*. They may affect performance and must be rejected. Friction, viscous forces and torques will be treated, unlike in [9], as unknown disturbances to be estimated and rejected.
(3) *Measured and known disturbances*. The traction speed v_t is measured, but acceleration a_t and jerk s_t are treated as unknown disturbances as in (11) and (12). The reference tension P is treated as in (13).
(4) *Web vibration modes*. They may affect closed-loop stability being neglected by the Embedded Model. They are time-varying due to reel radius and their damping may be uncertain due to variable web viscosity. Their range can be estimated from a simplified linear dynamics under extreme values of the reel radius. They must be confirmed by detecting vibration modes from simulation/plant tests.

By restricting detection of vibration modes to simulation, a simple test may be the harmonic analysis of the fine model subject to wide-band noise. The amplitude of the harmonic response from I to z_d, in m/A units, is shown in Fig. 2. The dashed line derives from a 16th order LTI approximation of Eqs. (6)–(10) as the result of assuming constant reel radius in (6). The solid line is the ratio between the dancer position PSD and the white noise PSD of the motor current. Responses differ at lower frequencies due to nonlinearity and at higher frequencies because of numerical errors. Fig. 2 shows four main vibrations due to web and motor gear.

3. The embedded model

The Embedded Model, written either in DT state equations or in Z-transform, is the baseline for designing digital control algorithms. It is a simplified version of the fine model, directly conceived in discrete time. Modal analysis as in Fig. 2, enhancing the principal modes, is a tool for fixing the state size of the controllable part.

3.1. Control requirements

Control requirements express the expected performance and the plant/environment scenario in which they must be met.

Table 2
Control requirements and constraints

Requirements	Variable	Symbol	Bound or tolerance	Unit
Disturbance	Traction speed	$0 \le v_t \le v_{t,\max}$	10	m/s
	Traction acceleration	$\lvert a_t T^{-2} \rvert \le a_{t,\max}$	2.5	m/s^2
Control performance	Dancer tracking error	$\lVert \underline{e}_d \rVert \le \varepsilon\left(\underline{z}_d\right)$	1[a]	mm
			2.5[b]	mm
Primary performance	Regulated web tension	$e_T = P - T_d$	200 ± 20	N
	Reel radius error	$\lvert \hat{e}_r = r - \hat{r} \rvert$	0.1	mm
Bounds	Reel radius	$0 < r_{\min} \le r \le r_{\max}$	$0.15 \div 0.6$	m
	Dancer (sensor range)	$\lvert z_d \rvert \le z_{d,\max}$	0.25	m
Control unit	Time unit	T	1/300	s

[a] At constant traction velocity.
[b] At variable traction velocity.

Although the primary performance should be web tension along the entire winding path, the latter is not directly measured and controlled in dancer roll plants. Therefore one must distinguish between control and primary performance, the former corresponding to some measured variable, such as the dancer position z_d. Control performance, corresponding to z_m in [10], drives control design and can be guaranteed a priori and assessed a posteriori from control measurements. For each performance variable, the reference trajectory class must be specified, together with a tolerance on the tracking error between reference and variable. Tolerance can be expressed through simple bounds as in Table 2 or by PSD profiles. Main performance variables are listed in Table 2 and their tracking errors are defined as follows.

(1) The dancer error is denoted as $\underline{e}_d = \underline{z} - z_m = \underline{z}_d - z_d$. The reference is the simplest one, i.e. $\underline{z}_d(i) = 0$, except for initial set-up from rest position. The requirement is expressed as

$$\left\lVert \underline{e}_d \right\rVert \le \varepsilon\left(\underline{z}_d\right). \tag{14}$$

(2) The regulated tension T_d is the total tension on the dancer roll; the relevant error is defined as $e_T = P - T_d$, where P is constant except during tension set-up.
(3) Reel radius error concerns the estimate $\hat{r}$ provided by control algorithms in Section 4.3.2 and is defined as $\hat{e}_r = r - \hat{r}$.

3.2. Embedded model

DT state equations and Z-transforms are represented by means of the following elements shown in Fig. 3.

(1) A DT integrator is denoted by a boxed Σ; it corresponds to $(z-1)^{-1}$.
(2) Constant or variable *gains* are enclosed in a circle and barred by an arrow when time-varying.
(3) *Arbitrary* input sources, the driving noise, are denoted by w and enclosed in a cloud.
(4) Z-transform formalism is used throughout, although affected by variable gains with r.

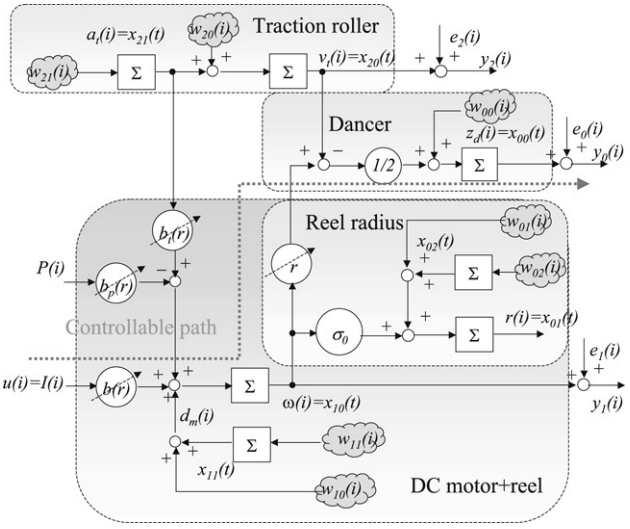

Fig. 3. Block diagram of the embedded model.

The EM derives from the following assumptions.

(1) *Time unit*. The time unit $T = 1/f_c$ is constrained by time resolution of DC motor suppliers for power range >10 kW, which implies $f_c \le 300$ Hz.
(2) *Ideal web*. Web is assumed perfectly rigid and adherent to rolls. It is a key assumption as all vibration modes of the fine model are accounted for as neglected dynamics. It implies (i) web tension is constant all along the web and that

$$T_0(t) = T_j(t) = 0.5\left(P(t) + m_d \dot{v}_d(t)\right), \quad j = 1, \ldots, 5 \tag{15}$$

holds, (ii) web speed downstream from the dancer becomes equal to reel tangential speed, the upstream speed becomes equal to the traction roller velocity, and their difference generates the vertical dancer motion, according to:

$$\begin{aligned} &\dot{x}_0(t) = v_0(t) = \cdots = v_2(t) \\ &v_3(t) = \cdots = v_6(t) = v_t(t) \\ &v_d(t) = 0.5\left(v_0(t) - v_t(t)\right) = 0.5\left(\omega(t)\, r(t) - v_t(t)\right). \end{aligned} \tag{16}$$

Then putting $x_{00} = z_d$ and converting (16) into discrete time the dancer equation follows:

$$x_{00}(i+1) = x_{00}(i) + (r(i)\,\omega(i) - v_t(i))/2 + w_{00}(i), \tag{17}$$

where the noise w_{00} accounts for deviations from the ideal web.

(3) *Ideal reel gear and DC motor drive*. The reel gear is treated as an ideal power transformer defined by $\omega_m = \tau\omega$. Accordingly, all major rotating and translating masses are added to the variable reel inertia J_r as follows

$$J(r) = J_r(r) + J_m\tau^2 + m_d r^2/4 \geq J(r_0) > 0. \tag{18}$$

The DC motor is assumed to be current-actuated so that $u = I$. By combining Eqs. (15), (16) and (18), the reel dynamics can be written as

$$\begin{aligned} x_{10}(i+1) &= x_{10}(i) + b(r)\,u(i) - b_p(r)\,P(i) \\ &\quad + b_t(r)\,a_t(i) + d_m(i), \end{aligned} \tag{19}$$

where $x_{10} = \omega = x\omega_r T$ is the reel angular increment, in radians, during T, d_m accounts for reel disturbance torques and the gains b, b_t and b_p are time-varying with r and equal to

$$\begin{aligned} &b(r) = \phi\tau T^2/J(r), \qquad b_p(r) = 0.5rT^2/J(r), \\ &b_t(r) = 0.25m_d r/J(r). \end{aligned} \tag{20}$$

(4) *Friction as unknown disturbance*. Viscous friction, roll eccentricity torques and reference uncertainties are encompassed by the single unknown disturbance d_m in (19). The latter is modeled as a first-order random process, as in Section 2.4:

$$\begin{aligned} &d_m(i) = w_{10}(i) + x_{11}(i), \\ &x_{11}(i+1) = x_{11}(i) + w_{11}(i). \end{aligned} \tag{21}$$

(5) *Reel radius dynamics*. Reel dynamics (19) must be completed with radius dynamics derived from (6)

$$\begin{aligned} x_{01}(i+1) &= x_{01}(i) + \sigma_0\omega(i) + x_{02}(i) + w_{01}(i) \\ x_{02}(i+1) &= x_{02}(i) + w_{02}(i), \end{aligned} \tag{22}$$

where $x_{01} = r$. The reel radius is driven by ω through the factor $\sigma_0 = 0.5\underline{s}/\pi$ proportional to mean web thickness $\underline{s}$ and by a first-order random disturbance accounting for web thickness uncertainty and variability.

(6) *Traction dynamics*. Traction speed v_t is modeled as in (11) and (12).

(7) *Output equations*. EM dynamics must be completed with equations relating model output $\mathbf{y}_m = \{y_{m0} = z_d, y_{m1} = \omega, y_{m2} = v_t\}$ to measures $\mathbf{y}^{\mathrm{T}} = \begin{bmatrix} y_0 & y_1 & y_2 \end{bmatrix}$, as defined in Section 2.1, less an error $\mathbf{e}$ accounting for measurement and model errors and defined by $\mathbf{y} = \mathbf{y}_m + \mathbf{e}$.

(8) *Performance variables*. Only z_d is accounted for, being the unique control performance, implying $z_m = z_d$.

Eqs. (17)–(22) can be collected into the following EM state equations

$$\begin{aligned} \left[\begin{array}{c} \mathbf{x}_c \\ \mathbf{x}_d \\ \hline \mathbf{x}_r \end{array}\right](i+1) &= \left[\begin{array}{cc|c} A_c(r) & H_c(r) & 0 \\ 0 & A_d & 0 \\ \hline 0 & 0 & A_r(\omega) \end{array}\right] \left[\begin{array}{c} \mathbf{x}_c \\ \mathbf{x}_d \\ \hline \mathbf{x}_r \end{array}\right](i) \\ &\quad + \left[\begin{array}{c} B_c(r) \\ 0 \\ \hline 0 \end{array}\right] u(i) + \left[\begin{array}{cc|c} G_c(r) & G_0(r) & 0 \\ G_d & 0 & 0 \\ \hline 0 & 0 & G_r \end{array}\right] \\ &\quad \times \left[\begin{array}{c} \mathbf{w} \\ P_0 \\ \hline \mathbf{w}_r \end{array}\right](i) \end{aligned} \tag{23}$$

$$\mathbf{y} = \begin{bmatrix} C_c & C_d \mid 0 \end{bmatrix}\mathbf{x}(i) + \mathbf{e}(i), z_m(i) = \begin{bmatrix} F_c & 0 \mid 0 \end{bmatrix}\mathbf{x}(i),$$

where radius dynamics (22) has been kept separate and reference tension P_0 (known disturbance) has been added. State variables and noise are defined by

$$\begin{aligned} &\mathbf{x}_c^{\mathrm{T}} = \begin{bmatrix} x_{00} & x_{10} \end{bmatrix}, \quad \mathbf{x}_d^{\mathrm{T}} = \begin{bmatrix} x_{11} & x_{20} & x_{21} \end{bmatrix}, \\ &\quad \mathbf{x}_r^{\mathrm{T}} = \begin{bmatrix} x_{01} & x_{02} \end{bmatrix} \\ &\mathbf{w}^{\mathrm{T}} = \begin{bmatrix} w_{00} & w_{10} & w_{11} & w_{20} & w_{21} \end{bmatrix}, \\ &\quad \mathbf{w}_r^{\mathrm{T}} = \begin{bmatrix} w_{01} & w_{02} \end{bmatrix}. \end{aligned} \tag{24}$$

Details of (23) can be found in [10] except for

$$\begin{aligned} &A_r(\omega) = \begin{bmatrix} \sigma_0\omega & 1 \\ 0 & 1 \end{bmatrix}, \qquad G_r = \begin{bmatrix} 1 & 0 \\ 0 & 1 \end{bmatrix}, \\ &G_0(r) = \begin{bmatrix} 0 \\ -b_p(r) \end{bmatrix}. \end{aligned} \tag{25}$$

3.3. EM eigenvalues, controllability and observability

All eigenvalues in (23) are unitary, which implies open-loop instability. Controllability and observability properties of (23), free of radius dynamics but time-varying, are the same as in [10], because reel radius never goes to zero, i.e. $0 < r_{\min} \leq r(i) \leq r_{\max}$ as reported in Table 2.

Proving observability of $\mathbf{x}_r$ is a bit more complex. As mentioned in [10], $\mathbf{y}_m$ has been designed oversized, which implies one entry out of $\mathbf{y}_m$, and specifically $y_{m0} = z_d$, to be committed observing $\mathbf{x}_r$ and z_d. Such a property derives from (17) being bilinear into r and ω. Extracting (17) and (22) from (23) and combining them into a single state equation yields

$$\begin{aligned} &\mathbf{x}_{dr}(i+1) = A_{dr}(\omega)\,\mathbf{x}_{dr}(i) + \mathbf{w}_{rd}(i) + H_{rd}\begin{bmatrix} v_t \\ \omega \end{bmatrix}(i) \\ &y_{m0} = C_{dr}\mathbf{x}_{dr}(i) \\ &\mathbf{x}_{dr} = \begin{bmatrix} x_{00} \\ x_{01} \\ x_{02} \end{bmatrix}, \qquad \mathbf{w}_{dr} = \begin{bmatrix} w_{00} \\ w_{01} \\ w_{02} \end{bmatrix}, \\ &A_{dr}(\omega) = \begin{bmatrix} 1 & \omega/2 & 0 \\ 0 & 1 & 1 \\ 0 & 0 & 1 \end{bmatrix}, \\ &H_{rd} = \begin{bmatrix} -1/2 & 0 \\ 0 & \sigma_0 \\ 0 & 0 \end{bmatrix}, \qquad C_{dr} = \begin{bmatrix} 1 & 0 & 0 \end{bmatrix}. \end{aligned} \tag{26}$$

Then the following result can be proved with the aid of [11].

Table 3
Peak of the fractional error dynamics

Type	Frequency [Hz]	Peak range [dB]	Radius range [m]	Web viscosity [N s]
Dancer	3.5	13 ÷ 20	0.15 ÷ 0.6	500 ÷ 1000
Reel	128 ÷ 150	58 ÷ 67	idem	idem

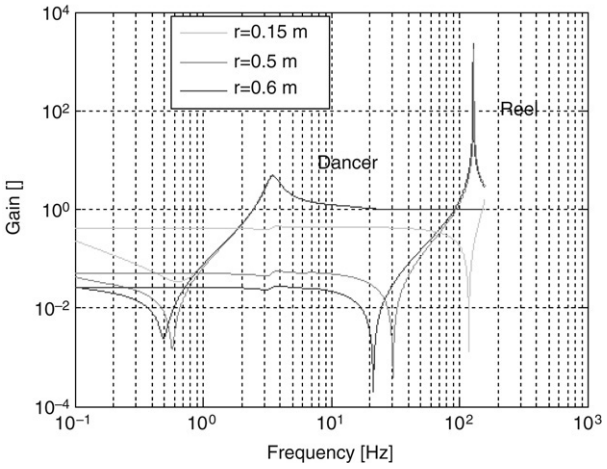

Fig. 4. Harmonic response of the dancer and reel error dynamics.

Result. The pair $(C_{dr}, A_{dr}(\omega))$ is observable if and only if $\omega(i) > 0$.

The above results show measures in (23) to be necessary and sufficient for observing all EM state variables, including $\mathbf{x}_r$, except when $\omega(i) = 0$, i.e. when the winding reel is blocked. The latter deficiency may create difficulties when the reel is replaced and the empty reel radius $r_{\min}$ must be refreshed. The solution is a bootstrap estimator as soon as $\omega(i) > 0$, not treated here.

3.4. The neglected dynamics

Treatment of neglected dynamics as outlined in [10] applies to web winding. Specifically:

(1) Only a pair of 'fractional error dynamics', $\partial\mathbf{P}_j$, $j = 0, 1$, affects closed-loop stability, namely dancer and reel, their harmonic amplitude being shown in Fig. 4 for different radius values.
(2) Both of them are combination of web and gear neglected vibrations and their harmonic amplitudes are dominated by the peak of the lowest frequency resonance. The peak range is reported in Table 3 versus radius and web viscosity variations.

4. Embedded model control

4.1. Introduction

Only tension regulation will be treated, and corresponds to zero tracking by dancer position. Actually EMC unifies all winding phases, from tension set-up to dancer zero

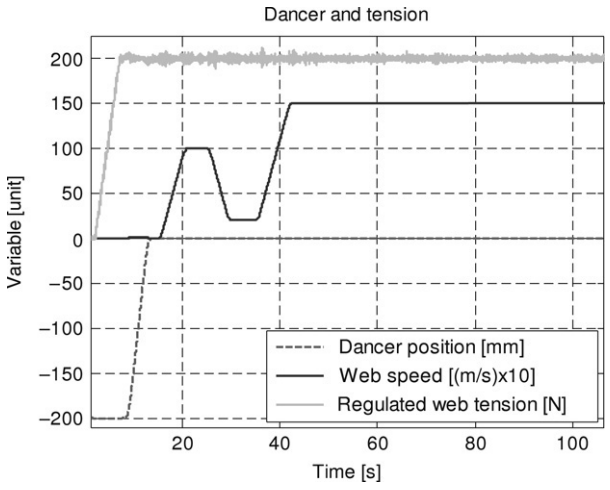

Fig. 5. Dancer zero acquisition and web tension/speed set-up.

acquisition and speed set-up, through a suitable hybrid Reference Generator. Typical profiles are shown in Fig. 5.

The Control Law makes the EM controllable states, here z_d and ω, to agree with their reference trajectories $\underline{z}_d$ and $\underline{\omega}$ by decoupling them from EM disturbance states.

4.2. Control law

4.2.1. Constant radius

The gain matrices $K(r)$, $Q(r)$ and $M(r)$ of the winder Control Law are derived in [10] under the assumption of constant radius. The resulting law, to be modified by state and radius estimates, is the following

$$\begin{aligned} u(i) = {} & \underline{u}(i) + k_0(r)\left(\underline{z}_d(i) - z_d(i)\right) \\ & + k_1(r)\left(\underline{\omega}(i) - \omega(i) + v_t(i)/r\right) \\ & - \left(z_m(i) + (b_t(r) - 1/r)\, a_t(i) - b_p(r)\, P_0(i)\right)/b(r). \end{aligned} \tag{27}$$

Eq. (27) has a clear physical meaning:

(1) the EM dancer position z_d tracks the reference $\underline{z}_d$ which is usually zero,
(2) the dancer position increment $r\omega - v_t$ [m] tracks the reference $r\underline{\omega}$ which is usually zero,
(3) the predictable reel disturbances, including known reference tension P_0, are exactly cancelled,
(4) $\underline{u}$ is the reference command whenever the dancer is moved from rest to zero or backward.

Q and M unequivocally derive from the EM; $K(r)$, defined by

$$K(r) = \left[2r^{-1}(1 - \lambda_{c0})(1 - \lambda_{c1}) \quad 2 - \lambda_{c0} - \lambda_{c1}\right]/b(r), \tag{28}$$

results from assigning the closed-loop spectrum $\Lambda_c = \{\lambda_{c0}, \lambda_{c1}\}$ inside the unit disk.

4.2.2. Extension to variable radius

The following result guarantees (27) and the corresponding gain matrices to asymptotically stabilize the closed-loop matrix $(A_c(r(i)) - B_c(r(i))\, K(r(i)))$ under variable radius.

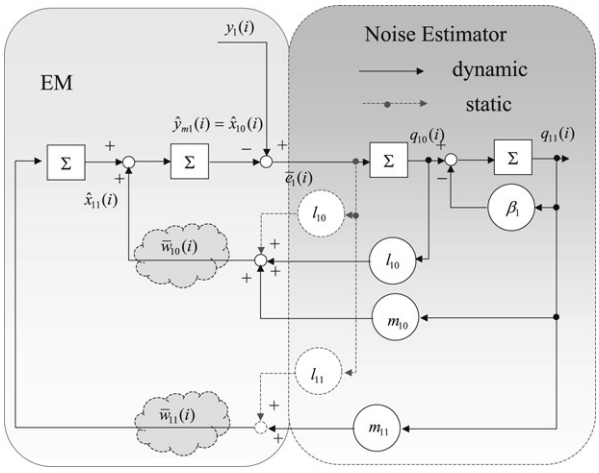

Fig. 6. Block diagram of the reel and traction observers showing static and dynamic noise estimators.

Result. Consider the controllable time-varying pair $(A_c(i), B_c(i))$ and assume there exists a pair of Lyapunov matrices [11] $(S(i), P(i))$ making the transformed pair

$$A_s = S(i)A_c\,(i)\,S^{-1}(i), \qquad B_s = S(i)B_c\,(i)\,P^{-1}(i) \tag{29}$$

controllable and time-invariant for any $i \geq 0$. Then there exists a feedback matrix K_s capable of fixing the spectrum Λ_s of $F_s = A_s - B_s K_s$ inside the unit disk. Constructing the feedback gain as $K\,(i) = P^{-1}\,(i)\,K_s S\,(i)$ ensures the equality

$$A_c(i) - B_c(i)P^{-1}\,(i)\,K_s S\,(i) = S^{-1}(i)\,(A_s - B_s K_s)\,S(i) \tag{30}$$

holds and consequently the spectrum is preserved, i.e. $\Lambda_c = \Lambda_s$.

The result applies to the winding case, since the matrix pair

$$S(i) = \begin{bmatrix} 1 & 0 \\ 0 & r\,(i) \end{bmatrix}, \qquad P(i) = r(i)b\,(r\,(i)) \tag{31}$$

is Lyapunov because of the bounded, non-zero radius r and command gain $b(r)$.

4.3. Noise estimators

Three separated Noise Estimators can be employed for real-time retrieving $\mathbf{w}(i)$ under constant radius. Each estimator may be designed as a static output-to-noise feedback, but two of them, reel and traction, need to be made dynamic to improve performance: (i) the reel estimator to increase gear vibration rejection close to the Nyquist frequency $f_{\max} = 0.5/T = 150$ Hz, (ii) the traction estimator to filter encoder quantization.

4.3.1. Reel and traction roller estimators

Rationale and mathematics are detailed in [10]. Fig. 6 shows the state observers arising from reel and traction EM as well as Noise Estimators in the static and dynamic configurations. Both of them, $j = 1, 2$, share the same block diagram except for the command channel u_j which is absent in the traction case, $j = 2$.

The feedback gains in Fig. 6 are reduced to minimum size, $n_j = 4$ in this case, to ensure that the closed-loop spectrum $\Lambda_{mj} = \{\lambda_{mj,0}, \ldots, \lambda_{mj,n_j-1}\}$ is freely and unequivocally assigned to the unit disk.

4.3.2. Dancer and reel radius observer

Consider the measure-driven decomposition of the EM pursued in [10] and replace the dancer dynamics, $j = 0$, with the time-varying dancer and radius dynamics in (26). According to Noise Estimator result in [10], a static feedback may be employed, since $n_0 = n_{w0} = 3$. However the resulting estimator must be time-varying and hybrid to cope with the observability deficiency as $\omega(i) \to 0$. To this end, a positive lower bound $\omega_{\min} > 0$ of $\omega(i)$ is designed, since only the winding process is treated. The estimator switches from full to partial feedback as follows:

$$\begin{bmatrix} \bar{w}_{00} \\ \bar{w}_{01} \\ \bar{w}_{02} \end{bmatrix}(i) = \begin{bmatrix} l_{00} \\ l_{01}/\hat{\omega}(i) \\ l_{02}/\hat{\omega}(i) \end{bmatrix} \bar{e}_0(i), \quad \text{if } \hat{\omega}(i) > \omega_{\min}$$
$$\begin{bmatrix} \bar{w}_{00} \\ \bar{w}_{01} \\ \bar{w}_{02} \end{bmatrix}(i) = \begin{bmatrix} m_{00} \\ 0 \\ 0 \end{bmatrix} \bar{e}_0(i), \quad \text{if } \hat{\omega}(i) \leq \omega_{\min}. \tag{32}$$

The variable gains in (32) depend on the estimate $\hat{\omega}(i)$ of the reel observer and guarantee that the closed-loop spectrum $\Lambda_{m0} = \{\lambda_{m0,0}, \lambda_{m0,1}, \lambda_{m0,2}\}$ is time-invariant and inside the unit disk when full feedback applies. In the case of partial feedback, $\lambda_{m0,1} = \lambda_{m0,2} = 1$ holds, implying that the radius is open-loop estimated and the estimation error $\hat{e}_r$ drifts for short times. The rate limit $\omega_{\min}$ is designed to bind $\hat{e}_r$ in the range s_0 of the web thickness during open-loop estimation as Section 4.4 shows. The state observer block diagram is shown in Fig. 7.

Fig. 8 shows the estimate $\hat{e}_r$ of the radius error, which is obtained by a bootstrap estimator during dancer set-up and ends for $t \geq 15$ s with an error of about 0.4 mm, less than 0.5%. The error is then brought close to or below the web thickness despite traction roller maneuvers as shown in Fig. 5.

4.4. Model-based closed-loop stability

Model-based closed-loop stability, i.e. under zero neglected dynamics, may be guaranteed as follows.

(1) In case of constant radius, the classical Separation Theorem applies requiring all closed-loop spectra to lie inside the unit disk.
(2) Section 4.2.2 allows a variable but known radius to be treated as the constant radius case.
(3) In case of variable and estimated radius, stability need to be proved, since Control Law becomes affected by radius error. The trick is to replace r with the estimate $\hat{r}$ in the Embedded Model (23) and in the subsequent EMC design, in which case Separation Theorem and the result of Section 4.2.2 hold. Of course, a model error arises, and must be included in the neglected dynamics. The latter is bounded by binding the radius error $\hat{e}_r$ as in Section 4.3.2.

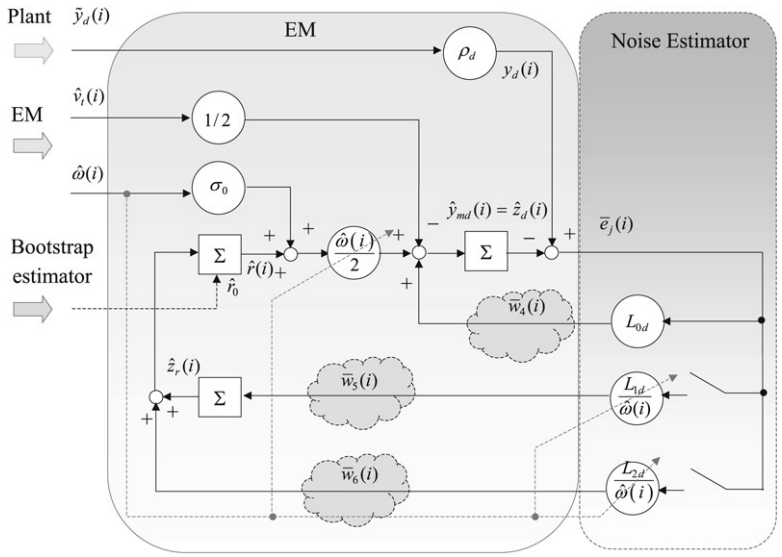

Fig. 7. Block diagram of the hybrid dancer and radius observer.

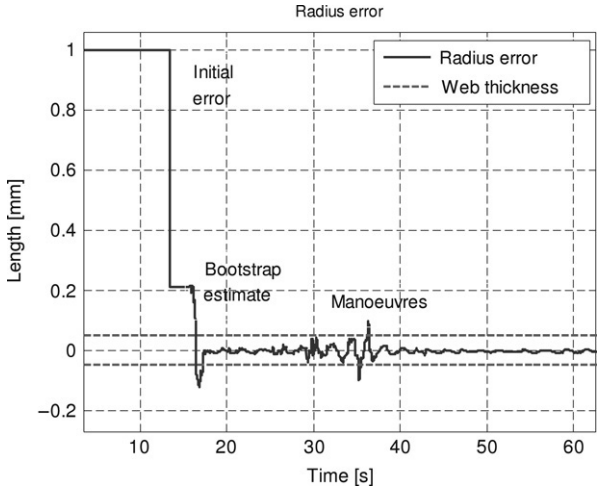

Fig. 8. Simulated radius estimation error at winding onset.

5. Eigenvalue tuning

Four eigenvalue sets must be tuned, namely Λ_c and $\{\Lambda_{m0}, \Lambda_{m1}, \Lambda_{m2}\}$. In the following, each spectrum will be assumed to have equal eigenvalues, denoted by λ_c and $\{\lambda_{m0}, \lambda_{m1}, \lambda_{m2}\}$ respectively. Tuning takes advantage of the error loop concept and formulation in [10]. Specifically, the design guidelines detailed there are followed.

5.1. Error loop inequalities

Consider the error loop inequalities in [10]:

(1) The robust stability inequality is shown there to hold

$$\max_{|f|\le f_{\max}} |(\mathbf{V}_{m0}\partial\mathbf{P}_0 + \mathbf{S}_{m0}\mathbf{V}_{m1}\partial\mathbf{P}_1)\,(\mathrm{e}^{j2\pi fT})| \le \eta < 1. \tag{33}$$

(2) The performance inequality is made explicit with respect to the measurement errors v_j. To this end, rewrite the EM errors $\hat{e}_j = y_{mj} - \hat{y}_{mj}$ already derived in [10]:

$$\begin{aligned}\hat{e}_0(z) &= -\mathbf{V}_{m0}(z)\,(\partial\mathbf{P}_0(z)\,y_{m0}(z) + v_0(z)) \\ &\quad + \mathbf{S}_{m0}(z)\,(z-1)^{-1}\,(w_0(z) \\ &\quad - r_t\hat{e}_2(z)/2 + r\hat{e}_1(z)/2) \\ \hat{e}_1(z) &= -\mathbf{V}_{m1}(z)\,(\partial\mathbf{P}_1(z)\,y_{m1}(z) + v_1(z)) + v_{e1}(z) \\ \hat{e}_2(z) &= -\mathbf{V}_{m2}(z)\,v_2(z) + v_{e2}(z)\,.\end{aligned} \tag{34}$$

Then, assuming $\underline{e}_d \simeq -\hat{e}_0$ to be guaranteed by inequality (38), assuming $\underline{z}_d = 0$ (dancer at zero position) and $\eta \ll 1$ in (33), it follows that

$$\begin{aligned}\underline{e}_d(z) &\simeq \mathbf{V}_{m0}(z)\,v_0(z) \\ &\quad - \mathbf{S}_{m0}(z)\,(z-1)^{-1}\left(-\hat{r}\mathbf{V}_{m1}(z)\,v_1(z)\right. \\ &\quad \left. + r_t\mathbf{V}_{m2}(z)\,v_2(z)\right)/2 + v_d(z)\,,\end{aligned} \tag{35}$$

where the disturbance components driven by $\mathbf{w}$ have been compacted into v_d. The relevant inequality, restricted to measurement errors, derives from (14) and holds

$$\begin{aligned}&\|\mathbf{V}_{m0}(z)\,n_0(z) - \mathbf{S}_{m0}(z)\,(-\mathbf{V}_{m1}(z)\,n_1(z) \\ &\quad + \mathbf{V}_{m2}(z)\,n_2(z))\,\| \le \gamma_d\varepsilon(0)\,,\end{aligned} \tag{36}$$

where $\gamma_d < 1$ leaves a margin for allocating v_d, and v_j has been replaced by errors in length units:

$$\begin{aligned}&n_0(z) = v_0(z)\,, \qquad n_1(z) = \hat{r}(z-1)^{-1}v_1(z)/2, \\ &n_2(z) = r_t(z-1)^{-1}v_2(z)/2.\end{aligned} \tag{37}$$

(3) The sensitivity inequality $|\mathbf{S}_c| \ll |\mathbf{S}_m|$ is converted, in [10], into a gap between Control Law and Noise Estimator eigenvalues, which can be rewritten here as

$$\delta\max\{(1-\lambda_{m0}),(1-\lambda_{m1})\} \le (1-\lambda_c) \le 1, \quad \delta > 1. \tag{38}$$

Only dancer and reel eigenvalues enter (38), since they are in charge of filtering neglected dynamics.

5.2. Reel and dancer eigenvalue tuning

Stability inequality (33) allows reel and dancer Noise Estimators to be tuned. To this end, (33) can be separated into a pair of inequalities, since the resonance peaks of $\partial \mathbf{P}_j$ are well frequency separated, as Fig. 4 and Table 3 show. Compute resonance peak and frequency as

$$\begin{aligned} &\max_{|f|\le f_{\max}} |\partial \mathbf{P}_j| \simeq \left(2\zeta_{j,\min}\right)^{-1} \\ &f_{j,\min} = \arg \max_{|f|\le f_{\max}} |\partial \mathbf{P}_j|, \end{aligned} \tag{39}$$

where damping and frequency have been minimized in order to be conservative. Taking the high frequency limit in (33), stability inequalities approximate to

$$\begin{aligned} &|\mathbf{V}_{m0}\left(jf_{0,\min}\right)| \simeq m_{00}\left(2\pi f_{0,\min}T\right)^{-1} \le 2\eta\zeta_{0,\min} \\ &|\mathbf{S}_{m0}\left(jf_{1,\min}\right)\mathbf{V}_{m1}\left(jf_{1,\min}\right)| \simeq l_{10}\left(2\pi f_{1,\min}T\right)^{-2} \\ &\qquad\qquad \le 2\eta\zeta_{1,\min}, \end{aligned} \tag{40}$$

where the Noise Estimator gains in (40) hold

$$l_{10} = 6\left(1-\lambda_{m1}\right)^2, \qquad m_{00} = 3\left(1-\lambda_{m0}\right). \tag{41}$$

Replacing (41) in (40) and solving for eigenvalues, provides the sufficient stability bounds

$$\begin{aligned} &\lambda_{m1} \ge 1 - 2\pi f_{1,\min}T\sqrt{\eta\zeta_{1,\min}/3} = \lambda_{m1,\min} \\ &\lambda_{m0} \ge 1 - 4\pi f_{0,\min}T\eta\zeta_{0,\min}/3 = \lambda_{m0,\min}. \end{aligned} \tag{42}$$

Note that (42) closely depends on damping, which is always very uncertain and could lead to quite conservative bounds. The only way to escape conservatism is to improve damping approximation by including hysteresis and friction losses, and then to rely on simulation and in-field refinement. The first trial bound is obtained at the stability limit, i.e. by setting $\eta = 1$, which yields

$$\lambda_{m0,\min} \cong 0.995, \qquad \lambda_{m1,\min} \cong 0.977. \tag{43}$$

5.3. Sensor design and traction roller eigenvalues

The second step is to guarantee performance through inequality (36). Due to several degrees-of-freedom, performance bound may be allocated to sensors in a uniform way, giving rise to three separate inequalities. Assuming v_j to be dominated by sensor quantization ρ_j, which implies $|n_j| \le \rho_j/2$, adopting the l_∞ norm and setting $\gamma_d = 1/2$ in (36), the following inequality derives with the aid of [12]

$$\rho_j \le \varepsilon(0)/3, \quad j = 0, 1, 2. \tag{44}$$

Then, quantization definition and notations in Section 2.1 yield the sensor design

$$\begin{aligned} &\mu_d \ge \log_2\left(2z_{d,\max}/\rho_0\right) \ge 10 \\ &N_r \ge 0.25\pi r_{\max}/\rho_1 \ge 1400 \\ &N_t \ge 0.25\pi r_t/\rho_2 \ge 500. \end{aligned} \tag{45}$$

Table 4
Winder eigenvalues

Set	Size	Designed	Simulated	Bandwidth (Hz)
Control unit	Nyquist frequency 150 Hz			
Control law	2	0.77×2	0.85×2	7.2
Dancer observer	3	0.995×3	0.992×2, 0.99	0.38
Reel observer	4	0.977×4	0.98×3, 0.96	0.96
Traction observer	4	0.97×4	0.94×3, 0.92	2.9

Table 5
Winder sensors

Variable (unit)	Sensor	Range	Division range	
			Designed	Simulated
Dancer (m)	LVDT	± 0.2	1024	1024
Traction roller (rad)	Encoder	$\pm\pi$	1400	1600
Reel (rad)	Encoder	$\pm\pi$	500	1600

Traction eigenvalues can be bounded as $\lambda_{m2} \ge 1 - \sigma_2$, upon definition of the signal-to-noise ratio $\sigma_2 = \sigma_{w2}/\sigma_{v2}$ between the standard deviations of disturbance and measurement noise, as in Kalman filter design [13]. Since Control Law (27) must include the traction acceleration a_t, taking $\sigma_{w2} = \gamma_2 a_{t,\max} T^2$ and employing Table 2, yield

$$\lambda_{m2} \ge 1 - \frac{\gamma_2 \alpha_{t,\max} T^2}{\rho_2/\sqrt{12}} \simeq 0.97, \quad \gamma_2 = 0.1. \tag{46}$$

5.4. Eigenvalue and sensor design summary

Refinement through simulator resulted in a slight modification of all eigenvalues, as shown in Table 4, where the bandwidth column refers to simulated values. Specifically:

(1) Control Law spectrum was slowed down to reduce command amplitude during maneuvers, a problem not treated here.
(2) Dancer spectrum was designed slightly conservative, because of the damping poor estimate, and made slightly faster in simulation.
(3) Reel spectrum was slowed down to better cope with the low-damped resonance of the gear.
(4) Traction spectrum was made faster to improve the estimate of v_t and a_t, acting as reference signals for winding. The same criterion led to a more accurate traction encoder as in Table 5.

Sensor quantization and range as imposed by requirements and design are reported in Table 5.

6. Simulated performance and comparison

6.1. Simulated performance

A summary of simulated performance is reported in Table 6. Bounds on absolute values of the most significant variables are compared to steady-state requirements from Table 2. Performance is separated into steady-state (constant web speed,

Table 6
Summary of simulated performance

Variable	Unit	Requirements: steady state (maneuvers)	Bound to absolute values	
			Steady state	Maneuvers
Tension error	N	20	10	10
Dancer error	mm	0.5 (2.5)	0.5	1.0
Radius error	mm	0.1	0.05	0.1

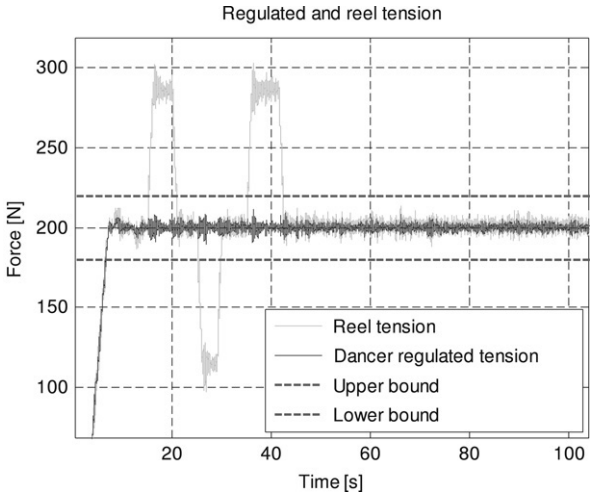

Fig. 9. Enlargement of Fig. 5 during onset maneuvers.

10 m/s) and onset/halt maneuvers (acceleration/deceleration). All requirements are met with a margin.

Fig. 9 shows the regulated and reel tensions during winding, together with bounds. Reel tension significantly diverges from regulated tension during maneuvers because of intermediate mass and friction. Jumps up and down reaching 100 N may be reduced by smoothing the traction velocity profile defined in Table 2.

Fig. 10 shows the dancer position and its tolerance during and after onset maneuvers. The actual simulated position (time-continuous) overlaps the digital measure, which oscillates around zero by a single bit. Obviously, dancer fluctuations closely correspond to the regulated tension in Fig. 9.

6.2. Comparison with published reports

A comparison with control schemes and laws reported in the literature is not straightforward, because very often web and winder parameters are not reported and test/measurement details are rather unclear. A more precise comparison could be achieved by implementing alternative schemes on the same simulator/plant, which is outside the scope of this paper. The trend, as in [9,14], is to accompany PID control with some kind of state observer for direct disturbance estimation and rejection. Different classical schemes are reported in [5], but only simulated responses of tension and dancer position to reference steps are shown, always affected by overshoot: here tension and dancer are brought smoothly to their reference values without any perceptible overshoot, as shown in Figs. 5 and 9. Other control laws from LQG to H_∞ are employed in [2–4].

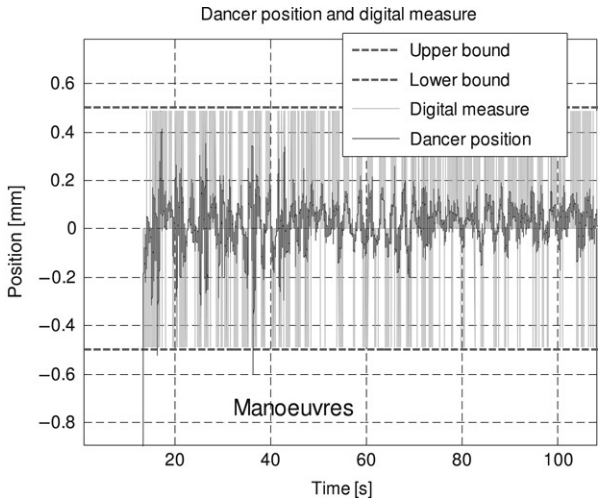

Fig. 10. Dancer position during and after onset maneuvers.

Table 7
Comparison with published reports

Case	Sensors	First resonance [Hz]	Acceleration [m/s^2]	Tension overshoot [%]	Type
This paper	Dancer, reel and traction encoders	3.5	<2.5	<5	Simulated
[9]	Load cell, reel encoder	>20	<1	>15	In-field
[3]	Load cell	>8	<1	>5	In-field

Comparable tests are repeated, web-velocity changes, as in Fig. 5. What emerges is a web tension overshoot, always greater than 5% ahead of web accelerations that are not greater than 1 m/s^2. Overshoot occurs at the beginning and end of acceleration/deceleration maneuvers, and is due to incoming web jerk, as imposed by the traction roller. A model-based disturbance estimate and rejection, sensitive to reel radius variation, as implemented by Noise Estimators (Section 4.3) and Control Law (Section 4.2) tries to conceal overshoot within high-frequency noise, as in Figs. 5 and 9, and ahead of web accelerations greater than 1 m/s^2 as reported in Table 2.

A more detailed comparison, shown in Table 7 has been attempted with [9,3]. In [9], tension control using load-cell and reel encoder is compared to an observer-based tension control. In both cases, the traction encoder only serves to regulate traction speed. Reel radius is open-loop estimated from the reel encoder. In [3], a pair of gain-scheduled control laws, based on the H_∞ technique, is compared. Tension in the winding section is controlled by the winding motor, employing load-cell measurement. No reel encoder is employed. Reel radius estimation is not mentioned. Table 7 shows the most favourable performance extracted from [9,3]. The first resonance value has been estimated from Bode plots in [9,3]. In summary, performances look rather comparable, as discrepancies might

be due to the actual traction jerks, which could not be estimated.

7. Conclusions

An end-to-end design of a model-based control unit for winding processes has been outlined. The methodology takes advantage of the process Embedded Model, which is the core of the control algorithms and involves the relevant interfaces from/to the plant: namely the Noise Estimator, part of the Measurement Law, and the Control Law. As the latter directly descends from the EM, no sophisticated algorithms are needed to tune their eigenvalues. A kind of hierarchical Separation Principle simplifies their tuning: Noise Estimator spectrum is constrained by neglected dynamics, Control Law spectrum is constrained by the Noise Estimator. Simulation and in-field tests allow them to be refined. When the EM, as in this case, is capable of covering a large process class, the same holds for the whole control unit, thus favouring standardization and reusability. Future directions are in-field experiments, and extension to load-cell sensors and more complex web handling processes.

Unlike model-based design, where little attention is paid to model parameters, which are either identified or their uncertainty accommodated by complex robust design, each model parameter has been carefully selected, reducing them to a minimum. This means for instance that disturbance dynamics is parameter-free, thus avoiding the effort and nuisance in parameter estimation often encountered in the literature. When parameters are significantly variable, as is the reel radius, they must be real-time estimated, which requires them to be observable and naturally leads EMC to become adaptive. As Control and Measurement Laws directly descend from the EM, their complexity is the same, which looks quite different from H_∞ techniques where complex and blind laws are obtained. Is this one of the reasons why control engineers still rely on PID control, where gains can be traced back to model and requirements? As the EMC tuneable gains are closed-loop eigenvalues, more or less as in LQG design, they are neatly related to EM and their values to requirements, as briefly shown in this paper. Usually no optimization is sought, which might involve other parameters, but it is simply sufficient to achieve the requirements.

As far as the authors are aware, the only drawback is a heavy modeling effort, passing through the fine model to be implemented as a numerical simulator and acting as a preliminary test-bench. The fine model is then simplified and split into EM, the core of the control architecture, and neglected dynamics, fixing the impenetrable wall to control performance. Unfortunately no automatic gear appears to be available, but only experience, intuition and perseverance.

References

[1] Ebler NA, Arnason R, Michaelis G, D'Sa N. Tension control: Dancer rolls or load cells. IEEE Trans Ind Appl 1993;29(4):727–39.
[2] Knittel D, Laroche E, Koç H. Tension control for winding systems with two degrees of freedom H_∞ control. In: Proc. ind. appl. conf., 36th IAS annual meeting, vol. 1. p. 576–82.
[3] Koç H, Knittel D, de Mathelin M, Abba G. Robust gain-scheduled control in web winding systems. In: Proc. 2000 IEEE conf dec control. p. 4116–9.
[4] Noura H, Bastogne T. Tension optimal control of a multivariable winding process. In: Proc. 1997 American control conf. p. 2499–503.
[5] Liu Z. Dynamic analysis of center-driven web winder controls. In: Conf. record of the 1999 IEEE ind. appl. conf., 34th IAS annual meeting, vol. 2. p. 1388–96.
[6] Hussian AE, et al. Modelling of a winding machine using genetic programming. In: Proc of the 2000 IEEE congress on evolutionary computation. p. 398–402.
[7] Sakamoto T, Tanaka S. Interaction measures for the decentralized tension control system. In: Proc. 2000 IEEE int. symp. on ind. electronics, vol. 2. p. 649–54.
[8] Young GE, Reid KN. Lateral and longitudinal dynamic behavior and control of moving webs. J Dyn Sys Meas Control 1993;115:309–17.
[9] Lin KC. Observer-based tension feedback control with friction and inertia compensation. IEEE Trans Control Syst Technol 2003;11(1):109–18.
[10] Canuto E. Embedded model control: Outline of the theory. ISA Trans 2007;46(3):363–77.
[11] Chen C-T. Linear system theory and design. New York: Holt, Rinehart & Winston; 1984.
[12] Desoer CA, Vidyadsagar M. Feedback systems: Input–output properties. New York: Academic; 1975.
[13] Kwakernaak H, Sivan R. Linear optimal control systems. New York: Wiley; 1972.
[14] Hou Y, Gao Z, Jiang F, Boulter BT. Active disturbance rejection control for web tension regulation. In: Proc. 40th IEEE conf on decision and control. 2001, p. 4974–9.

Enrico Canuto was born in Varallo (Piemonte), Italy. He received the degree in Electrical Engineering from Politecnico di Torino. In 1983 he joined Politecnico di Torino, Torino, Italy, as Associate Professor of Automatic Control. He contributed from 1982 to 1997 to data reduction of the European astrometric mission Hipparcos. Since 1998 he developed Embedded Model Control (EMC) as a way of equalizing design, implementation and maintainance. Technological studies in view of scientific and drag-free space missions, like GAIA, GOCE, LISA, … were the occasion of applying Embedded Model Control to electro-optics. EMC applications to industrial control are in process. His research interests cover the whole field of challenging control problems because of complexity, uncertainty and precision.

Fabio Musso was born in Casale Monferrato, Italy. He received the "Laurea" degree in electrical engineering and the Ph.D. degree in information and system engineering from Politecnico di Torino, Turin, Italy. He is now with Alcatel Alenia Space Italia, Turin, Italy, involved in the Nanobalance project funded by European Space Agency: a sub-micronewton interferometric thrust-stand. His research interest include automation, control and data elaboration in the electro-optics field.